Scilight

Translational Insights

https://www.sciltp.com/journals/ti

Article

Cognition-Weighted Multimodal MRI and FDG-PET Features for Classification of Mild Cognitive Impairment, Alzheimer's Disease, and Frontotemporal Dementia

Sunil Kumar Khokhar [1,2], Rohit Misra [3], Manoj Kumar [1], Faheem Arshad [4], Nithin Thanissery [4], Sandeep Kumar [4], Tejaswini Manae [4], Subasree Ramakrishnan [4], Mohammad Haris [2], Sandhya Mangalore [1], Suvarna Alladi [4], Tapan Kumar Gandhi [3] and Rose Dawn Bharath [1,*]

[1] Department of Neuroimaging and Interventional Radiology, National Institute of Mental Health and Neurosciences, Bengaluru 560029, India
[2] Department of Radiology, University of Pennsylvania, Philadelphia, PA 19104, USA
[3] Department of Electrical Engineering, Indian Institute of Technology Delhi, New Delhi 110016, India
[4] Department of Neurology, National Institute of Mental Health and Neurosciences, Bengaluru 560029, India
* Correspondence: cns.researchers@gmail.com

How To Cite: Khokhar, S.K.; Misra, R.; Kumar, M.; et al. Cognition-Weighted Multimodal MRI and FDG-PET Features for Classification of Mild Cognitive Impairment, Alzheimer's Disease, and Frontotemporal Dementia. *Translational Insights* **2026**, *1*(1), 11. https://doi.org/10.53941/ti.2026.100011

Received: 5 April 2026
Revised: 31 May 2026
Accepted: 3 June 2026
Published: 10 July 2026

Abstract: Background: Differentiating between mild cognitive impairment (MCI), Alzheimer's disease (AD), and frontotemporal dementia (FTD) subtypes remains a clinical challenge due to overlapping cognitive symptoms, structural atrophy, and metabolic patterns, particularly in the early stages. Machine learning approach integrating with multimodal neuroimaging and cognitive scores may offer early, accurate classification and, subsequently, improved diagnostic precision. Methods: In this study, we included 100 participants (50 AD, 30 FTD [14 behavioral variant FTD (bvFTD) and 16 primary progressive aphasia (PPA)], and 20 MCI) who underwent simultaneous structural MRI and FDG-PET imaging. Cortical thickness (CTH) from structural MRI and standardized uptake values from FDG-PET were extracted using FreeSurfer and PETSurfer pipelines, respectively. ACE-III scores were used to derive a logistic weighting function that assigns relative weights to FDG-PET metabolic features and structural cortical-thickness features on a per-region basis, with greater metabolic weighting at lower ACE-III scores reflecting the established earlier emergence of metabolic decline. A Naive Bayes classifier was trained on the merged features, and performance was evaluated using repeated stratified five-fold cross-validation. Results: The model achieved classification accuracies of 81% for MCI vs. dementia (AD + FTD), 80% for MCI vs. AD, 78% for MCI vs. FTD, 86% for MCI vs. PPA, 77% for MCI vs. bvFTD, and 70% for AD vs. FTD. The overall classification accuracy was 64%, with the highest discriminative performance observed in separating MCI from PPA. Conclusions: This study presents a novel, cognition-weighted multimodal approach combining structural and metabolic imaging to enhance the classification of neurodegenerative syndromes. Findings from this study underscore the potential of integrating ACE-III scores with neuroimaging biomarkers to accurately characterize and differentiate early-stage MCI, AD, and FTD subtypes, although further validation in larger cohorts is required.

Keywords: multimodal neuroimaging; cortical thickness; FDG-PET; logistic weighting; dementia classification; naive bayes classifier

1. Introduction

Alzheimer's disease (AD) is the most common cause of dementia, whereas frontotemporal dementia (FTD) represents an important cause of early-onset dementia [1]. FTD presents clinically as variants, including the behavioral variant FTD (bvFTD) with behavioral and executive dysfunctions [2,3], and primary progressive aphasia (PPA) encompassing the semantic variant PPA (svPPA) characterized by semantic anomalies and comprehension deficits, and non-fluent/agrammatic variant PPA (nfvPPA), impairing speech, grammar, and word production [4]. AD is characterized by progressive memory loss and contributes significantly to cognitive impairment [5]. Early detection and precise identification of these neurodegenerative conditions, including their prodromal phase, mild cognitive impairment (MCI) [6,7], are critical for early diagnosis and management [8].

Neuroimaging techniques such as magnetic resonance imaging (MRI) and [18-F] Fluorodeoxyglucose Positron emission tomography (FDG-PET) provide adjunctive value in the diagnosis of Dementias, although interpretation largely depends on the expertise of the clinician [9,10]. Novel advances in quantitative neuroimaging enable advanced analysis of cortical morphometry and cerebral metabolic alterations. Previous studies showed the medial temporal and parietotemporal atrophy in AD, while FTD syndromes exhibit atrophy in the frontal, anterior temporal, and fronto-insular cortices [4,11–13]. bvFTD typically exhibits pronounced atrophy in the anterior cingulate and frontal insular cortices, whereas nfv-PPA presents atrophy predominantly in the left frontal region, including the inferior frontal gyrus, pars triangularis, rolandic operculum, and precentral gyrus. svPPA is characterized by distinctive atrophy primarily in the left anterior temporal lobe, which distinguishes it from other FTD syndromes [4]. However, delineating these different dementia types presents a challenge due to the subtlety of early-stage FTD cortical atrophy and overlapping atrophy characteristics across FTD syndromes, AD, and MCI. Machine learning (ML) algorithms have gained momentum for the classification and prediction of diverse neurodegenerative disorders [14,15].

Previous studies on neurodegenerative disease classification, particularly regarding AD and FTD, has witnessed significant advancements through the integration of imaging biomarkers and cortical thickness (CTH) measures [16,17]. One notable study explored the effectiveness of cerebrospinal fluid (CSF) and MRI biomarkers across a spectrum of neurodegenerative diseases [18]. It highlighted significant differences in imaging variables, including hippocampal and amygdalar volumes and CTH, across different clinical diagnoses, supporting the utility of these biomarkers in clinical practice beyond AD and MCI groups [18,19]. In another study, a hierarchical classification model of FTD was developed using ML approaches to assess the CTH. The research used the Small Univalue Segment Assimilating Nucleus (SUSAN) technique to reduce noise, thereby enhancing the clarity and reliability of the imaging data. This model achieved significant accuracy, with the best performance observed with the support vector machine (SVM) approach, illustrating the potential of ML-driven methods to improve the diagnostic predictability of neurodegenerative diseases [20]. Furthermore, a study on ML-based hierarchical classification demonstrated the potential of CTH data to differentiate between FTD, AD, and their subtypes [21]. The use of noise-reducing techniques and a structured hierarchical classification approach yielded an overall accuracy of 75.8%; the classification accuracies of CN vs. Dementia, AD vs. FTD, and bvFTD vs. PPA were 86.1%, 90.8%, and 86.9%, respectively [21]. This approach not only enhanced classification accuracy but also provided critical insights into the regional patterns of neurodegeneration, paving the way for targeted interventions [21]. Other studies on the classification of AD patients from CN subjects showed accuracies of 92.35% and 91.50%, and of MCI from AD at 75.90% [22,23].

Despite these advances, most prior approaches assign uniform or unsupervised weights to imaging features and do not explicitly account for the stage-dependent contributions of structural and metabolic change. The present study introduces a cognition-weighted strategy in which the ACE-III score is used, through a logistic function, to determine the relative contribution of CTH and FDG-PET features on a per-region basis before classification with a Naive Bayes model. The objective of this study was to evaluate whether ACE-III-based logistic weighting of simultaneously acquired MRI-derived cortical thickness and FDG-PET features could improve the classification of MCI, AD, and FTD subtypes using a Naive Bayes classifier. Performance was assessed using accuracy, sensitivity, specificity, and the area under the receiver operating characteristic curve (AUC-ROC). These findings underscore the potential of ML-based, cognition-weighted multimodal imaging for the early and more accurate classification of MCI, AD, bvFTD, and PPA.

2. Methods

2.1. Participants

In this ambispective comparative cohort study, we investigated a total of one hundred patients with dementia, comprising 50 individuals with AD, 20 with MCI, and 30 with FTD. The FTD group had two subgroups: 14 with

the bvFTD and 16 with PPA. Participants with incomplete data, motion-corrupted MRI, FreeSurfer/PETSurfer reconstruction failures, or major incidental structural abnormalities were excluded prior to analysis. The severity of dementia was assessed using the Clinical Dementia Rating (CDR) scale. Cognitive evaluations were conducted using ACE-III [24], which encompassed domains such as memory, attention, language, fluency, and visuospatial skills. The diagnosis of FTD was made in patients using the standard criteria [2,4], and AD was diagnosed in patients who fulfilled the NIA-AA (National Institute on Aging and Alzheimer's Association) criteria for probable and possible AD [25], while the diagnosis of MCI was made based on the modified Petersen criteria [26]. This study received approval from the institute's ethics committee [Ethics NO. NIMH/DO/(BS&NS DIV.) 2019-20].

There were no significant between-group differences in age, duration of illness, or education level ($p > 0.05$). However, differences were observed in the ACE scores and their subdomain scores among the groups. The mean ACE scores for MCI, AD, FTD-BV, and PPA were 87.3 (SD = 5.53), 46.02 (SD = 20.61), 52.57 (SD = 18.79), and 33.56 (SD = 21.09), respectively. These differences were statistically significant ($p < 0.001$). Post hoc Bonferroni tests (Supplementary Table S1) showed that scores in the MCI group were significantly higher than those of all other groups ($p < 0.01$). Additionally, bvFTD showed significantly higher ACE scores in the language subdomain compared with PPA, whereas fluency and language scores were significantly lower in PPA than in AD (Table 1). The participants in this study were the same cohort as those included in the previously reported AD and FTD studies [27,28], and thus, the acquisition protocols and behavioral assessments were consistent across all studies.

Table 1. Demographic and Cognitive Characteristics of Participants.

	MCI		**AD**		**FTD**				**F/χ^2**	***p*-Value**
					bvFTD		**PPA**			
N	20		50		14		16			
Sex (M:F)	15:05		23:27		09:05		05:11		8.57	0.036
	Mean	SD	Mean	SD	Mean	SD	Mean	SD		
Age	61.40	8.22	63.50	9.54	66.64	8.30	58.69	7.26	2.24	0.09
Duration of illness (years)	2.42	2.20	2.94	1.71	3.18	1.38	2.75	0.98	0.71	0.55
Education	15.40	3.12	13.62	4.97	14.14	4.59	13.94	4.17	0.74	0.53
ACE-III	87.30	5.53	46.02	20.61	52.57	18.79	33.56	21.09	28.51	<0.001
Attention	16.44	2.01	8.58	4.39	11.62	3.80	6.87	4.47	21.50	<0.001
Memory	21.11	3.34	8.02	5.85	10.31	5.92	6.33	5.62	29.14	<0.001
Fluency	9.83	2.50	5.12	3.15	5.46	2.47	2.80	2.31	18.71	<0.001
Language	25.22	1.63	16.80	6.76	19.00	5.67	11.40	7.95	14.43	<0.001
Visuospatial	14.39	2.59	6.90	4.65	8.15	4.20	5.53	4.12	16.64	<0.001

Abbreviations: MCI—Mild cognitive impairment, AD—Alzheimer's Disease, FTD—Frontotemporal dementia, bvFTD—behaviour FTD, PPA—Primary Progressive Aphasia, ACE-III—Addenbrooke's Cognitive Examination-III, SD—standard deviation; M:F—Male:Female; Between-group differences were tested with ANOVA (continuous variables) and the chi-square test (sex).

2.2. Acquisition Parameters

2.2.1. MRI

All participants underwent structural magnetic resonance imaging (sMRI) using a 3 Tesla clinical MRI (Biograph mMR) scanner (Siemens, Erlangen, Germany) equipped with a 16-channel head coil. To minimize head movement and enhance patient comfort during the scan, the head was stabilized with foam pads. The imaging process included a 3D T1-weighted Magnetization Prepared Rapid Acquisition Gradient-Recalled Echo (MPRAGE) sequence with 192 sections and a repetition time (TR) of 2300 ms, echo time (TE) of 2.42 ms, slice thickness: 1 mm, flip angle of 9°, a field of view (FOV) of 250 × 250 mm, a matrix resolution of 256 × 256. In addition, other sequences such as Fluid-Attenuated Inversion Recovery (FLAIR), T2-weighted imaging, and Susceptibility Weighted Imaging (SWI) were employed as part of the routine diagnostic MRI scan, and also ensured the exclusion of structural abnormalities in all patients.

2.2.2. FDG-PET

All participants received an intravenous bolus injection of 185 ± 10% MBq (approximately 5.0 mCi) of [18F]-FDG 30 minutes prior to scan acquisition, and imaging was performed in list mode for 15 minutes. These images had a resolution of 256 matrices, a 300 mm field of view, and voxel dimensions of 2.3 mm × 2.3 mm × 5 mm. using fully 3D or Fourier-rebinned Ordered Subset Expectation Maximization (OSEM) iterative reconstruction

algorithms with three iterations and 35 subsets. Standard corrections for attenuation, scatter, random coincidences, and decay were applied, as well as a 5 mm Gaussian post-reconstruction filter.

2.3. Image Processing

2.3.1. Cortical Thickness

The cortical reconstruction and estimation of CTH were performed using the FreeSurfer image analysis tool v6.05 [29] (Available online: https://surfer.nmr.mgh.harvard.edu (accessed on 15 September 2023)). The pipeline within the FreeSurfer suite involves automated motion correction, skull stripping, automated transformation onto Talairach space, subcortical white matter and gray matter segmentation, and tessellation of gray matter and white matter boundaries. Next, the cortical surface was reconstructed by high-resolution inter-subject alignment procedures to yield a high-resolution quantification of CTH, along with differentiation into different atlas-derived and prescribed cortical brain regions [30]. The Desikan-Killiany (DK) atlas was used for the parcellation of the cortical surface into distinct units based on gyral and sulcal anatomy, with 34 regions per hemisphere [31].

2.3.2. FDG-PET

The FDG-PET image processing was performed using the PETSurfer analysis tool v6.05 [32]. The process started by utilizing on the FreeSurfer results from the MPRAGE images to enable PET processing (Figure 1). This involved registering into a standardized template space and applying the Partial Volume Correction (PVC) using geometric transfer matrix (GTM) techniques to address partial volume effects [33]. After segmentation and registration, PETSurfer computed SUV values using the pons as a reference region, calculated the region volume, and measured voxel variance. We then used a 10 mm full-width half maximum (FWHM) Gaussian filter to smooth the FDG-PET images. We also applied the DK atlas to parcel the cortical surface into 34 regions per hemisphere [31].

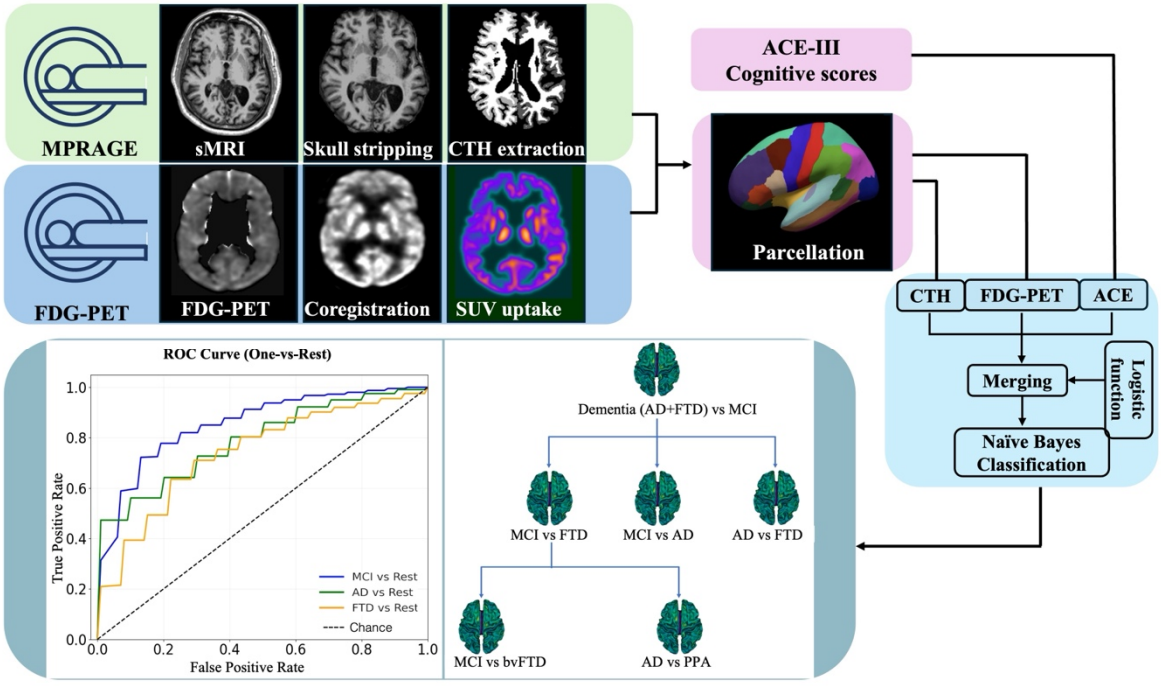

Figure 1. Demonstrating integration of multimodal MRI and FDG-PET processing and classification pipeline. MPRAGE and FDG-PET images were processed for CTH and SUV extraction, respectively. ACE-III cognitive scores and parcellated regions were integrated with imaging data using a logistic weighting function. A Naive Bayes model classified MCI, AD, and FTD, with performance shown via ROC curves.

2.4. Machine Learning-Based Classifications

We used the scikit-learn library for ML classification in a Jupyter notebook (Python v3.7.3) to implement ML classification algorithms [34]. A Naive Bayes classifier was used to classify MCI, AD, and FTD from the cognition-weighted merged CTH/FDG-PET feature vector. The merged feature vector was used directly as input to the classifier.

Naive Bayes

Naive Bayes is a supervised algorithm based on certain "naive" assumptions that predictors in a model are independent of each other. Though unrealistic in a real-world scenario, this simplistic model simplifies probability calculations and enables the algorithm to run quickly and efficiently. Despite this simplifying assumption, Naive Bayes often provides good results, especially for large datasets with many features.

$$P(xi\ |y) = \frac{1}{\sqrt{2\pi}\sigma_y^2}\exp\left(-\frac{\left(x_i - u_y\right)^2}{2\sigma_y^2}\right) \quad (1)$$

where: $P(xi\ |y)$—represents the probability of a feature x_i given class of y; u_y—is the mean of feature x_i for class y; $2\sigma_y^2$—is the variance of feature x_i for class y.

The term $\frac{1}{\sqrt{2\pi}\sigma_y^2}$ is the normalization factor of the Gaussian distribution. The exponential term $\exp\left(-\frac{(x_i-u_y)^2}{2\sigma_y^2}\right)$ calculates the probability density of x_i for a Gaussian distribution with a mean u_y and variance σ_y^2. The parameters, σ_y and u_y are estimated using maximum likelihood.

2.5. Cross-Validation and Preprocessing

Model performance was evaluated using repeated stratified k-fold cross-validation (k = 5, 20 repeats), which preserved class proportions in each fold given the imbalanced subgroup sizes. Feature standardization and computation of the ACE-III-derived logistic weights were performed within each cross-validation fold using statistics estimated on the training partition only; the corresponding test partition was transformed using these parameters to prevent data leakage.

2.6. Cognition-Weighted Feature Merging

Weight's function was defined to accept an input from ACE scores and compute the weights CTH and FDG-PET using a logistic function. The logistic function was applied to each ACE score element to calculate the corresponding FDG-PET value. The CTH values were calculated as 1 minus the FDG-PET values. The CTH and FDG-PET weights were calculated for each element of the ACE scores using the weight function. A merged array was initialized with the same shape as data CTH. The algorithm iterated through each region of interest (ROI) from 0 to 67. For each ROI of CTH was standardized by subtracting the mean and dividing by the standard deviation, while FDG-PET ROIs were also standardized in the same manner. The resulting products were added together to create the merged data for each ROI. Finally, merged two sets of data, CTH and FDG-PET, using the weights derived from ACE for CTH and FDG-PET.

2.7. Logistic Function

A logistic function was used to map normalised ACE scores to cognition-dependent weights.

$$f(x) = \frac{L}{1 + \exp(-(\mathrm{ACE} - 0.5))} \quad (2)$$

where: ACE score was normalised for 0 to 1. L = the curve's maximum value.

2.8. Statistical Analysis

Statistical analysis was performed with '*scipy'* library in Python. Between-group differences in age, education, and ACE-III scores were tested using an analysis of variance (ANOVA) for continuous variables, and gender differences were tested using a chi-square test. Post-hoc analyses using Bonferroni-corrected pairwise *t*-tests, following a Kruskal-Wallis test for the ordinal variable CDR, were conducted to examine pairwise group differences at the 0.05 significance level.

3. Results

The Naive Bayes classifier was implemented for classifying three dementia classes: MCI, AD, and FTD. The model's accuracy was 0.64, indicating that in 64% of instances, it correctly classified these conditions (Table 2). The area under the receiver operating characteristic curve (AUC-ROC) score for MCI was 0.85, for AD was 0.79,

and for FTD was 0.74 (Figure 2). The sensitivity for MCI, AD, and FTD was 0.75, 0.72, and 0.40, respectively, while the specificity for these classes was 0.81, 0.70, and 0.90, respectively (Table 2).

Table 2. Performance metrics of the Naive Bayes classifier for the three-class model (MCI vs. AD vs. FTD).

Metric	MCI	AD	FTD
Accuracy		0.64	
AUC-ROC score	0.85	0.79	0.74
Sensitivity	0.75	0.72	0.40
Specificity	0.81	0.70	0.90

Overall multiclass accuracy.

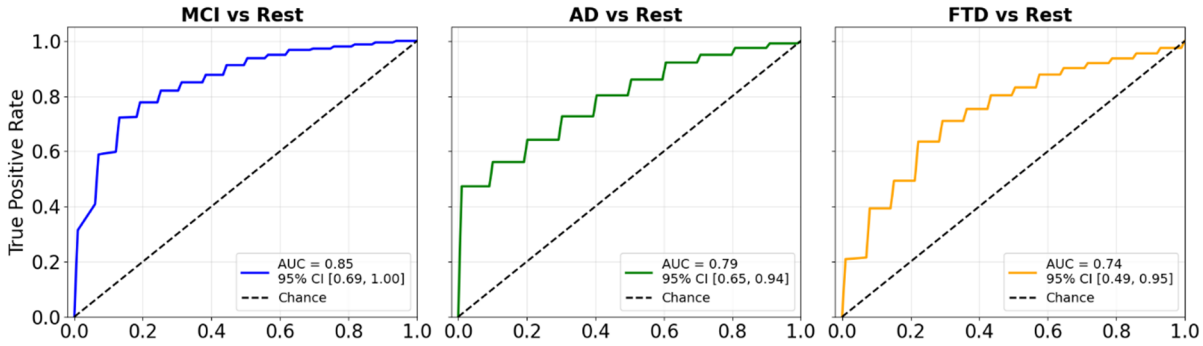

Figure 2. The figure displays the ROC curve for the One-vs-Rest approach.

3.1. Diagnostic Classification Metrics for the One vs. Rest

Subsequently, the Naive Bayes classifier was evaluated on its ability to distinguish MCI from Dementia (AD and FTD combined), MCI from AD, MCI from FTD, MCI from bvFTD, and MCI from PPA. The AUC-ROC scores, accuracy, sensitivity, and specificity for each classification task are provided in Table 3.

Table 3. Classification performance of the Naive Bayes model across diagnostic tasks.

Classification	AUC-ROC Score	Accuracy	Sensitivity	Specificity
MCI vs. Dementia (AD + FTD)	0.82	0.81	0.83	0.75
AD vs. FTD	0.76	0.70	0.57	0.78
MCI vs. AD	0.87	0.80	0.82	0.75
MCI vs. FTD	0.81	0.78	0.80	0.75
MCI vs. bvFTD	0.76	0.77	0.71	0.80
MCI vs. PPA	0.87	0.86	0.88	0.85

Abbreviations: MCI—Mild cognitive impairment, AD—Alzheimer's Disease, FTD—Frontotemporal dementia, bvFTD—behaviour FTD, PPA—Primary Progressive Aphasia, AUC-ROC—Receiver Operating Characteristic-Area Under the Curve.

3.2. Diagnostic Classification Metrics for the One vs. One

Figure 3 shows the results of ROC curves MCI vs. Dementia and their subtypes. When distinguishing between MCI and a combined group of AD and FTD, the classifier had an AUC-ROC score of 0.82, an accuracy of 0.81, a sensitivity of 0.83, and a specificity of 0.75. This suggests that the classifier is quite capable of differentiating between these conditions. In differentiating MCI from AD specifically, the classifier achieved an AUC-ROC of 0.87, an accuracy of 0.80, a sensitivity of 0.82, and a specificity of 0.75. The model was reasonably good at identifying and differentiating these conditions, though not as proficient as with the combined group. The classifier showed performance in differentiating between MCI and FTD, with an AUC-ROC of 0.81, accuracy of 0.78, sensitivity of 0.80, and specificity of 0.75. This indicates a relatively good ability to discriminate between these two conditions. Differentiating MCI from bvFTD yielded an AUC-ROC of 0.76, accuracy of 0.77, sensitivity of 0.71, and specificity of 0.80. The results collectively suggest an effective discrimination between MCI and bvFTD. Finally, when the task was to differentiate MCI from PPA, the classifier achieved an AUC-ROC of 0.87, an accuracy of 0.86, a sensitivity of 0.88, and a specificity of 0.85 (Table 3). This indicates the classifier is highly capable of distinguishing between these two conditions.

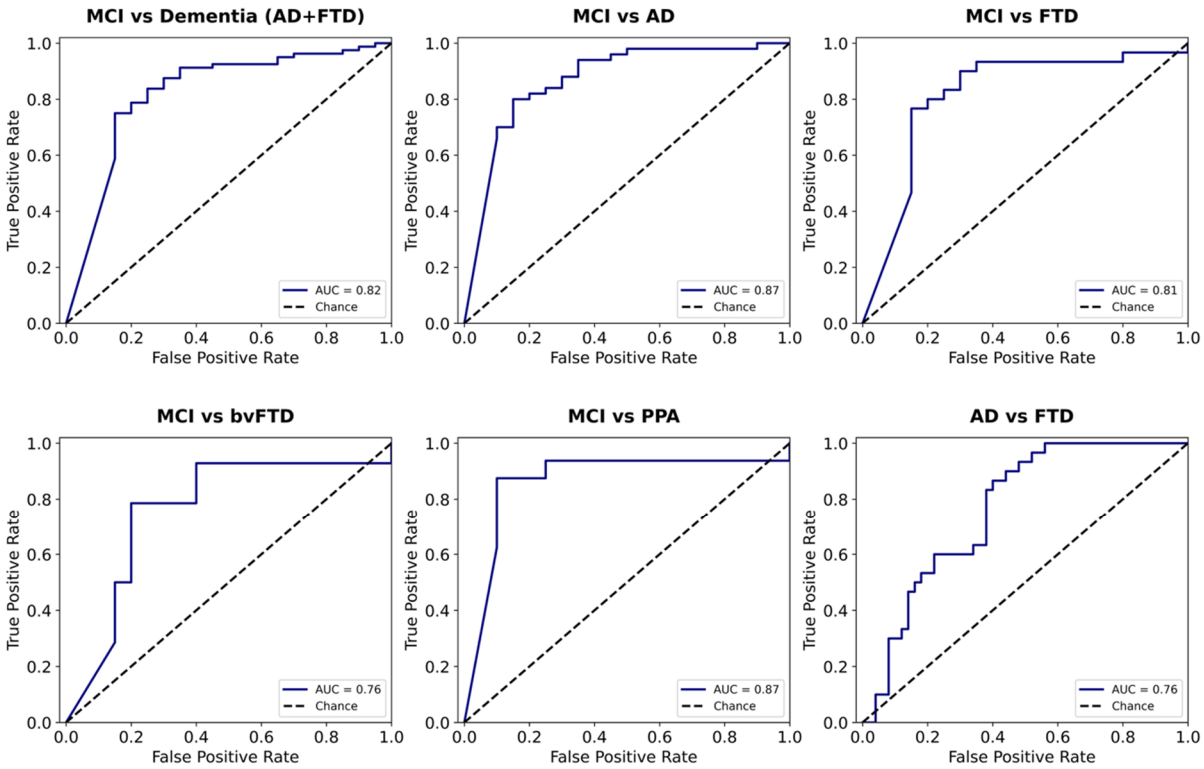

Figure 3. ROC curves depicting the discriminative ability of the Naive Bayes classifier in differentiating MCI from various dementia types (AD, FTD, bvFTD, PPA).

4. Discussion

In this study, we introduce a novel approach for classifying dementia subtypes by integrating CTH from structural MRI, SUV uptake values from FDG-PET, and cognitive assessment using the ACE-III, and further using a Naive Bayes classifier with a logistic function-based weighting function. Our results underscore the diagnostic utility of combining structural, metabolic, and cognitive biomarkers, particularly in differentiating MCI from AD and FTD subtypes. The classifier achieved its highest accuracy in differentiating MCI from PPA at 86%, with 78% accuracy for MCI versus FTD overall, and 81% accuracy when distinguishing MCI from all combined dementia groups (AD and FTD). These results (Table 3) support the diagnostic advantage of combining structural, metabolic, and cognitive biomarkers over any single modality alone. These findings bring into line with previous evidence that FDG-PET provides greater sensitivity for early metabolic dysfunction, while cortical atrophy measured by CTH complements spatial specificity to later-stage degeneration [35,36]. The hybrid model's performance supports recent advances in multimodal neuroimaging that emphasize the added value of combining structural and functional data for early differential diagnosis [28,37,38].

A distinguishing feature of our approach is the usage of ACE-III scores not merely as a covariate but as a biologically motivated weighting function that modulates the relative contribution of imaging features during classification. This method models the non-linear trajectory of neurodegeneration and reflects growing evidence that cognitive decline correlates with the convergence of multiple neuropathological processes [39,40]. Unlike traditional models with static or uniform feature weighting, our biologically motivated framework captures the progressive and heterogeneous nature of dementia. Machine learning approaches have gained considerable traction in neurodegenerative disorders research, with support vector machines, random forests, and deep neural networks demonstrating strong performance across various classification tasks [41]. However, these methods typically demand large scale, well-curated training datasets and involve extensive hyperparameter optimization, both of which pose practical challenges in clinical neuroimaging contexts where sample sizes are often limited. Naive Bayes classifiers, by contrast, are computationally simple and provide transparent probabilistic outputs. Their assumption of feature independence, although idealized, has been shown to be effective in neuroimaging classification tasks with limited sample sizes [42]. Our results confirm that Naive Bayes performs robustly in high-dimensional, low-sample contexts and is well-suited for translational research.

A central contribution of this study is the use of a logistic function applied to ACE-III scores to derive weights for imaging features. This biologically motivated approach reflects the disease continuum, in which declining cognitive performance is increasingly influenced by metabolic deficits, thereby enhancing the physiological

relevance of data fusion. Unlike traditional multimodal models that often rely on equal or unsupervised feature weighting [38,43], our method provides a flexible, scalable mechanism for integrating cognition-weighted biomarkers. The use of a Naive Bayes classifier, though less common than support vector machines and deep learning models, proved efficient and interpretable. Despite its simplifying assumption of feature independence, it offered robust performance in a high-dimensional, small-sample context, consistent with earlier studies demonstrating its effectiveness in related domains [42,44,45]. Notably, the classifier's specificity in differentiating MCI from both bvFTD and PPA reached above 80%, suggesting strong potential to rule out false positives in early clinical screening.

However, moderate sensitivity in distinguishing AD from FTD (57%) likely reflects the heterogeneity within the whole cohort, including early-stage or atypical presentations that overlap of clinical symptoms with other subtype of dementias [46]. The overlap in structural and metabolic patterns between AD and FTD subtypes, especially in the frontal cortex, poses a well-known diagnostic challenge [47]. Future models may benefit from ensemble classifiers or non-linear approaches such as gradient boosting and neural networks that better capture these complex overlaps.

Limitations

This study has few limitations. First, the sample size was modest, particularly for the FTD subtypes (bvFTD, n = 14; PPA, n = 16), so metrics that depend on these small subgroups should be interpreted cautiously. Second, the study lacked an independent external validation cohort; the reported performance therefore requires confirmation in separate datasets. Finally, longitudinal designs assessing diagnostic stability over time would strengthen the clinical utility of this framework and allow prediction of disease progression.

5. Conclusions

This study supports the feasibility of cognition-weighted integration of structural MRI and FDG-PET features for dementia classification. The approach showed promising performance for selected comparisons, particularly MCI versus FTD subtypes. Larger independent and longitudinal studies are needed to establish generalizability and clinical utility. Future work should explore integrate additional biomarkers, such as CSF tau/Aβ, plasma NfL, or digital phenotyping, to further refine early diagnosis and personalized care pathways.

Supplementary Materials

The additional data and information can be downloaded at: https://media.sciltp.com/articles/others/2607101015439571/TI-26040045-SI.pdf.

Author Contributions

S.K.K.: Conceptualization, Data curation, Formal analysis, Methodology, Software, Visualization, Writing—original draft preparation, Writing—review and editing. R.M.: Methodology, Formal analysis, and Validation. M.K.: Supervision, Validation, Writing—review and editing. F.A.: Data curation, Investigation, Resources, Validation, Writing—review and editing. N.T.: Data curation, and Methodology. S.K.: Data curation, Validation. T.M.: Data curation, Validation. S.R.: Data curation, Supervision. M.H.: Methodology, Validation, Writing—review and editing. S.M.: Methodology, Resources, Writing—review and editing. S.A.: Conceptualization, Data curation, Supervision, Validation, Writing—review and editing. T.K.G.: Conceptualization, Methodology, Supervision, Validation, Writing—review and editing. R.D.B.: Conceptualization, Investigation, Methodology, Resources, Supervision, Validation, Writing—review and editing. All authors have read and agreed to the published version of the manuscript.

Funding

This research received no specific grant from any funding agency in the public, commercial, or not-for-profit sectors. The authors independently conducted the study, and all necessary resources and materials were provided by National Institute of Mental Health and Neurosciences.

Institutional Review Board Statement

The study was conducted according to the guidelines of the Declaration of Helsinki, and approved by the Institutional Ethics Committee of the National Institute of Mental Health and Neurosciences (NIMHANS), Bengaluru, India. The approval number is [Ethics NO. NIMH/DO/(BS&NS DIV.) 2019-20]. dated 23/01/2020.

Informed Consent Statement

Informed consent was obtained from all subjects involved in the study.

Data Availability Statement

Data from the current study are not publicly available due to conditions of our ethics approval, particularly regarding patient confidentiality, and do not permit public archiving of the original data but are available from the corresponding author on reasonable request.

Conflicts of Interest

The authors declare no conflict of interest.

Use of AI and AI-Assisted Technologies

During the preparation of this work, the authors used Grammarly in order to check grammar and clarity. After using this tool, the authors reviewed and edited the content as needed and take full responsibility for the content of the published article.

References

1. Grossman, M.; Seeley, W.W.; Boxer, A.L.; et al. Frontotemporal Lobar Degeneration. *Nat. Rev. Dis. Primers* **2023**, *9*, 40. https://doi.org/10.1038/s41572-023-00447-0.
2. Rascovsky, K.; Hodges, J.R.; Knopman, D.; et al. Sensitivity of Revised Diagnostic Criteria for the Behavioural Variant of Frontotemporal Dementia. *Brain* **2011**, *134*, 2456–2477. https://doi.org/10.1093/brain/awr179.
3. Younes, K.; Miller, B.L. Neuropsychiatric Aspects of Frontotemporal Dementia. *Psychiatr. Clin. N. Am.* **2020**, *43*, 345–360. https://doi.org/10.1016/j.psc.2020.02.005.
4. Gorno-Tempini, M.L.; Hillis, A.E.; Weintraub, S.; et al. Classification of Primary Progressive Aphasia and Its Variants. *Neurology* **2011**, *76*, 1006–1014. https://doi.org/10.1212/WNL.0b013e31821103e6.
5. Russo, M.J.; Bueri, J.; Alba-Ferrara, L.; et al. Recognition Memory in Individuals with Mild Cognitive Impairment and Alzheimer's Dementia: A Systematic Review. *Appl. Neuropsychol. Adult* **2026**, 1–21. https://doi.org/10.1080/23279095.2025.2610375.
6. Albert, M.S.; DeKosky, S.T.; Dickson, D.; et al. The Diagnosis of Mild Cognitive Impairment Due to Alzheimer's Disease: Recommendations from the National Institute on Aging-Alzheimer's Association Workgroups on Diagnostic Guidelines for Alzheimer's Disease. *Alzheimers Dement.* **2011**, *7*, 270–279. https://doi.org/10.1016/j.jalz.2011.03.008.
7. Petersen, R.C.; Roberts, R.O.; Knopman, D.S.; et al. Mild Cognitive Impairment: Ten Years Later. *Arch. Neurol.* **2009**, *66*, 1447–1455. https://doi.org/10.1001/archneurol.2009.266.
8. Dubois, B.; von Arnim, C.A.F.; Burnie, N.; et al. Biomarkers in Alzheimer's Disease: Role in Early and Differential Diagnosis and Recognition of Atypical Variants. *Alzheimers Res. Ther.* **2023**, *15*, 175. https://doi.org/10.1186/s13195-023-01314-6.
9. Finger, E.C. Frontotemporal Dementias. *Continuum* **2016**, *22*, 464–489. https://doi.org/10.1212/CON.0000000000000300.
10. Foster, N.L.; Heidebrink, J.L.; Clark, C.M.; et al. FDG-PET Improves Accuracy in Distinguishing Frontotemporal Dementia and Alzheimer's Disease. *Brain* **2007**, *130*, 2616–2635. https://doi.org/10.1093/brain/awm177.
11. Herholz, K.; Westwood, S.; Haense, C.; et al. Evaluation of a Calibrated 18F-FDG PET Score as a Biomarker for Progression in Alzheimer Disease and Mild Cognitive Impairment. *J. Nucl. Med.* **2011**, *52*, 1218–1226. https://doi.org/10.2967/jnumed.111.090902.
12. Ou, Y.-N.; Xu, W.; Li, J.-Q.; et al. FDG-PET as an Independent Biomarker for Alzheimer's Biological Diagnosis: A Longitudinal Study. *Alzheimers Res. Ther.* **2019**, *11*, 57. https://doi.org/10.1186/s13195-019-0512-1.
13. Qiao, Z.; Wang, G.; Zhao, X.; et al. Neuropsychological Performance Is Correlated with Tau Protein Deposition and Glucose Metabolism in Patients with Alzheimer's Disease. *Front. Aging Neurosci.* **2022**, *14*, 841942.
14. Cuingnet, R.; Gerardin, E.; Tessieras, J.; et al. Automatic Classification of Patients with Alzheimer's Disease from Structural MRI: A Comparison of Ten Methods Using the ADNI Database. *NeuroImage* **2011**, *56*, 766–781. https://doi.org/10.1016/j.neuroimage.2010.06.013.
15. Ito, K.; Fukuyama, H.; Senda, M.; et al. Prediction of Outcomes in Mild Cognitive Impairment by Using 18F-FDG-PET: A Multicenter Study. *J. Alzheimers Dis.* **2015**, *45*, 543–552. https://doi.org/10.3233/JAD-141338.
16. Illán-Gala, I.; Falgàs, N.; Friedberg, A.; et al. Diagnostic Utility of Measuring Cerebral Atrophy in the Behavioral Variant of Frontotemporal Dementia and Association with Clinical Deterioration. *JAMA Netw. Open* **2021**, *4*, e211290. https://doi.org/10.1001/jamanetworkopen.2021.1290.

17. Pérez-Millan, A.; Lal-Trehan Estrada, U.M.; Falgàs, N.; et al. The Cortical Asymmetry Index for Subtyping Dementia Patients. *Eur. Radiol.* **2025**, *35*, 4713–4721. https://doi.org/10.1007/s00330-025-11400-y.
18. Pérez-Millan, A.; Thirion, B.; Falgàs, N.; et al. Beyond Group Classification: Probabilistic Differential Diagnosis of Frontotemporal Dementia and Alzheimer's Disease with MRI and CSF Biomarkers. *Neurobiol. Aging* **2024**, *144*, 1–11. https://doi.org/10.1016/j.neurobiolaging.2024.08.008.
19. Kaipainen, A.; Jääskeläinen, O.; Liu, Y.; et al. Cerebrospinal Fluid and MRI Biomarkers in Neurodegenerative Diseases: A Retrospective Memory Clinic-Based Study. *J. Alzheimers Dis.* **2020**, *75*, 751–765. https://doi.org/10.3233/JAD-200175.
20. Poonam, K.; Guha, R.; Chakrabarti, P.P. Artificial Intelligence Based Hierarchical Classification of Frontotemporal Dementia. In Proceedings of the 2024 46th Annual International Conference of the IEEE Engineering in Medicine and Biology Society (EMBC), Orlando, FL, USA, 15–19 July 2024; pp. 1–4.
21. Kim, J.P.; Kim, J.; Park, Y.H.; et al. Machine Learning Based Hierarchical Classification of Frontotemporal Dementia and Alzheimer's Disease. *NeuroImage Clin.* **2019**, *23*, 101811. https://doi.org/10.1016/j.nicl.2019.101811.
22. Wee, C.-Y.; Yap, P.-T.; Zhang, D.; et al. Identification of MCI Individuals Using Structural and Functional Connectivity Networks. *NeuroImage* **2012**, *59*, 2045–2056. https://doi.org/10.1016/j.neuroimage.2011.10.015.
23. Westman, E.; Muehlboeck, J.-S.; Simmons, A. Combining MRI and CSF Measures for Classification of Alzheimer's Disease and Prediction of Mild Cognitive Impairment Conversion. *NeuroImage* **2012**, *62*, 229–238. https://doi.org/10.1016/j.neuroimage.2012.04.056.
24. Mekala, S.; Paplikar, A.; Mioshi, E.; et al. Dementia Diagnosis in Seven Languages: The Addenbrooke's Cognitive Examination-III in India. *Arch. Clin. Neuropsychol.* **2020**, *35*, 528–538. https://doi.org/10.1093/arclin/acaa013.
25. McKhann, G.M.; Knopman, D.S.; Chertkow, H.; et al. The Diagnosis of Dementia Due to Alzheimer's Disease: Recommendations from the National Institute on Aging-Alzheimer's Association Workgroups on Diagnostic Guidelines for Alzheimer's Disease. *Alzheimers Dement.* **2011**, *7*, 263–269. https://doi.org/10.1016/j.jalz.2011.03.005.
26. Petersen, R.C. Mild Cognitive Impairment as a Diagnostic Entity. *J. Intern. Med.* **2004**, *256*, 183–194. https://doi.org/10.1111/j.1365-2796.2004.01388.x.
27. Khokhar, S.K.; Kumar, M.; Kumar, S.; et al. Alzheimer's Disease Is Associated with Increased Network Assortativity: Evidence from Metabolic Connectivity. *Brain Connect.* **2023**, *13*, 610–620. https://doi.org/10.1089/brain.2023.0024.
28. Khokhar, S.K.; Kumar, M.; Arshad, F.; et al. Multiplex Connectomics Reveal Altered Networks in Frontotemporal Dementia: A Multisite Study. *Netw. Neurosci.* **2025**, *9*, 615–630. https://doi.org/10.1162/netn_a_00448.
29. Fischl, B. FreeSurfer. *NeuroImage* **2012**, *62*, 774–781. https://doi.org/10.1016/j.neuroimage.2012.01.021.
30. Dale, A.M.; Fischl, B.; Sereno, M.I. Cortical Surface-Based Analysis. I. Segmentation and Surface Reconstruction. *NeuroImage* **1999**, *9*, 179–194. https://doi.org/10.1006/nimg.1998.0395.
31. Desikan, R.S.; Ségonne, F.; Fischl, B.; et al. An Automated Labeling System for Subdividing the Human Cerebral Cortex on MRI Scans into Gyral Based Regions of Interest. *NeuroImage* **2006**, *31*, 968–980. https://doi.org/10.1016/j.neuroimage.2006.01.021.
32. Greve, D.N.; Svarer, C.; Fisher, P.M.; et al. Cortical Surface-Based Analysis Reduces Bias and Variance in Kinetic Modeling of Brain PET Data. *NeuroImage* **2014**, *92*, 225–236. https://doi.org/10.1016/j.neuroimage.2013.12.021.
33. Greve, D.N.; Salat, D.H.; Bowen, S.L.; et al. Different Partial Volume Correction Methods Lead to Different Conclusions: An (18)F-FDG-PET Study of Aging. *NeuroImage* **2016**, *132*, 334–343. https://doi.org/10.1016/j.neuroimage.2016.02.042.
34. Pedregosa, F.; Varoquaux, G.; Gramfort, A.; et al. Scikit-Learn: Machine Learning in Python. *J. Mach. Learn. Res.* **2011**, *12*, 2825–2830.
35. Herholz, K.; Ebmeier, K. Clinical Amyloid Imaging in Alzheimer's Disease. *Lancet Neurol.* **2011**, *10*, 667–670. https://doi.org/10.1016/S1474-4422(11)70123-5.
36. Jack, C.R., Jr.; Bennett, D.A.; Blennow, K.; et al. NIA-AA Research Framework: Toward a Biological Definition of Alzheimer's Disease. *Alzheimers Dement.* **2018**, *14*, 535–562. https://doi.org/10.1016/j.jalz.2018.02.018.
37. Bi, S.; Chen, Z.; Tao, W.; et al. Multimodal Imaging for Diagnosis of Frontotemporal Dementia Using Integrated PET/MR. *J. Nucl. Med.* **2024**, *65*, 241923.
38. Venugopalan, J.; Tong, L.; Hassanzadeh, H.R.; et al. Multimodal Deep Learning Models for Early Detection of Alzheimer's Disease Stage. *Sci. Rep.* **2021**, *11*, 3254. https://doi.org/10.1038/s41598-020-74399-w.
39. Lawry Aguila, A.; Lorenzini, L.; Janahi, M.; et al. Deep Normative Modelling Reveals Insights into Early-Stage Alzheimer's Disease Using Multi-Modal Neuroimaging Data. *Alzheimers Res. Ther.* **2025**, *17*, 107. https://doi.org/10.1186/s13195-025-01753-3.
40. Marinescu, R.V.; Eshaghi, A.; Lorenzi, M.; et al. DIVE: A Spatiotemporal Progression Model of Brain Pathology in Neurodegenerative Disorders. *NeuroImage* **2019**, *192*, 166–177. https://doi.org/10.1016/j.neuroimage.2019.02.053.
41. Wang, Y.; Liu, S.; Spiteri, A.G.; et al. Understanding Machine Learning Applications in Dementia Research and Clinical Practice: A Review for Biomedical Scientists and Clinicians. *Alzheimers Res. Ther.* **2024**, *16*, 175. https://doi.org/10.1186/s13195-024-01540-6.

42. Moradi, E.; Pepe, A.; Gaser, C.; et al. Machine Learning Framework for Early MRI-Based Alzheimer's Conversion Prediction in MCI Subjects. *NeuroImage* **2015**, *104*, 398–412. https://doi.org/10.1016/j.neuroimage.2014.10.002.
43. Sadiq, M.U.; Kwak, K.; Dayan, E. Model-Based Stratification of Progression along the Alzheimer Disease Continuum Highlights the Centrality of Biomarker Synergies. *Alzheimers Res. Ther.* **2022**, *14*, 16. https://doi.org/10.1186/s13195-021-00941-1.
44. Kubi, N.N.B.A.; Nazir, S. Dementia Prediction with Multimodal Clinical and Imaging Data. *Int. J. Inf. Technol.* **2025**, *17*, 5–16. https://doi.org/10.1007/s41870-024-02326-7.
45. Zhang, D.; Wang, Y.; Zhou, L.; et al. Multimodal Classification of Alzheimer's Disease and Mild Cognitive Impairment. *NeuroImage* **2011**, *55*, 856–867. https://doi.org/10.1016/j.neuroimage.2011.01.008.
46. Vogel, J.W.; Young, A.L.; Oxtoby, N.P.; et al. Four Distinct Trajectories of Tau Deposition Identified in Alzheimer's Disease. *Nat. Med.* **2021**, *27*, 871–881. https://doi.org/10.1038/s41591-021-01309-6.
47. Musa, G.; Slachevsky, A.; Muñoz-Neira, C.; et al. Alzheimer's Disease or Behavioral Variant Frontotemporal Dementia? Review of Key Points Toward an Accurate Clinical and Neuropsychological Diagnosis. *J. Alzheimers Dis. JAD* **2020**, *73*, 833–848. https://doi.org/10.3233/JAD-190924.